Ontogeny of a synaptophysin-mediated GABA transmission mechanism from the ciliary band-associated strand to the ciliary band during the development of the sea urchin *Hemicentrotus pulcherrimus*

Hideki Katow[1,2*], Hiromi Yoshida[2], Tomoko Katow[1,], and Masato Kiyomoto[3,]

Short Title: Synaptophysin in GABA transmission

Affiliations:
[1]Division of Developmental Biology, Research Center for Marine Biology, Tohoku University, Aomori, Japan, [2]Center of Research Instruments, Institute of Development, Aging and Cancer, Tohoku University, Sendai, Japan, [3] Marine and Coastal Research Center, Ochanomizu University, Chiba, Japan

*Corresponding author:
Dr. Hideki Katow, Research Center for Marine Biology, Tohoku University, Asamushi, Aomori, Aomori 039-3501, Japan
Phone and facsimile: +81-17-741-3194

E-mail addresses:
Hideki Katow: hkatow@m.tohoku.ac.jp
Hiromi Yoshida. hiromi.yoshida.a6@tohoku.ac.jp
Masato Kiyomoto: kiyomoto.masato@ocha.ac.jp
Tomoko Katow: h.tkatow@d6.dion.ne.jp

PeerJ Preprints | https://doi.org/10.7287/peerj.preprints.26625v1 | CC BY 4.0 Open Access | rec: 6 Mar 2018, publ: 6 Mar 2018

Abstract

Swimming activity of the sea urchin larva depends on ciliary beating primarily in the circumoral ciliary band (CB) and is regulated by several neurotransmitters, such as 5HT, dopamine and γ-aminobutyric acid (GABA). Accordingly, the larval swimming activity is severely inhibited by 3-mercaptopropionic acid [a glutamate decarboxylase (GAD) inhibitor]. Although GABA is detected in the CB, GAD is absent. GAD is expressed in the spatially segregated nearby ciliary band-associated strand (CBAS). Thus, it is assumed that GABA transmission extends from the CBAS to the CB. Here, we examined the synaptic transmission mechanism by focusing on the spatiotemporal expression pattern of synaptophysin (Syp), a synaptic vesicle glycoprotein. The sea urchin has a single copy of the Syp gene, which encodes a 266-amino acid protein with possibly 4 transmembrane domains. We generated an anti-Syp antibody (Ab). Immunoblotting (IB) detected Ab binding to a single band at approximately 38 kDa. Whole-mount immunohistochemistry (WMIHC) detected high intensity Ab binding to the CBAS. Syp was initially detected at the mesenchyme blastula stage (mBL) as a single band by IB. Accordingly, WMIHC detected Syp in the cytoplasm of small patches of several ectodermal cells at the mBL stage. Syp has also been detected in the cytoplasm of blastocoelar cells from the prism stage to the 2-arm pluteus stage (2aPL). By the 4aPL stage, Syp was expressed in the CBAS and was moderately expressed among the blastocoelar cells. Distinctive co-localization of GABA and Syp was not detected until the 2aPL stage. Beginning at the 4aPL stage, GABA was detected in the CB and Syp-positive puncta in the CBAS. In the CB, GABA was co-localized with the GABA-A receptor ($GABA_AR$). Thus, the GABA signal may be transmitted from GAD in the CBAS through a Syp-mediated system to the CB and then, in the CB, to the basal body of the cilia through $GABA_AR$.

Keywords:

Sea urchin, CBAS, GABA, synaptophysin, immunohistochemistry

Introduction

The larval swimming activity of the sea urchin depends on ciliary beating in the ciliary band (CB) (*Mogami et al., 1991; Strathmann & Gru□nbaum, 2006*). The ciliary beating is regulated by various neurotransmitters, including 5HT (*Soliman 1983; Yaguchi et al., 2000; Yaguchi & Katow, 2003*), dopamine (*Soliman, 1983; Katow et al., 2010*), and γ-aminobutyric acid (GABA) (*Soliman, 1983; Katow et al., 2013*). GABA is detected in the CB of plutei *(Katow et al., 2013*); however, its synthetase glutamate decarboxylase (GAD) is not expressed in the CB. GAD is expressed in a subpopulation of the blastocoelar cells and the ciliary band-associated strand (CBAS) in plutei (*Katow et al., 2013; 2014; 2016; Katow, 2015*). GABA expression in the CB is severely inhibited by 3-mercaptopropionic acid (3-MPA), a GAD activity inhibitor (*Katow et al., 2013*), suggesting that GABA expressed in the CB is transmitted from the CBAS. Furthermore, our previous report of GABA-A receptor ($GABA_AR$) expression in the CB (*Katow et al., 2013*) provides mechanistic support for GABA localization in the CB.

Our previous ultrastructural analysis of the CBAS by transmission electron microscopy (TEM) detected groups of numerous cytoplasmic vesicles, including synaptic vesicles (SV) in the cytoplasm (*Katow et al., 2016*). The major membrane component of these endoplasmic vesicles (EV) is synaptophysin (Syp) (*McMahon et al., 1996; Sethi et al., 2013*). The CBAS contains numerous Syp-immunoreactive puncta (*Katow et al., 2016*), suggesting neurosecretory activity of the organ. In addition to the sea urchin, Syp has been reported in vast phylogenetic groups of invertebrates, such as the flatworm (*Schistosoma mansoni; Rabelo et al., 1997*), *C. elegans* (*Abraham et al., 2011*), insects (*Calábria, et al., 2011; Stevens et al., 2012*), *Aplysia* (*Jin et al., 2011*) and *Octopus* (*Zhang et al., 2012*).

In mammalian cells, GABA is packed in secretory vesicles after its synthesis by GAD (*Teng et al.,* 2013). Thus, the previous observations suggest that GABA transmission from the CBAS to the CB is mediated by the SV. Here, we report a further immunochemical analysis of GABA transmission in the ciliary beating-mediated larval swimming activity and the ontogenetic spatiotemporal expression patterns of Syp in the sea urchin *Hemicentrotus pulcherrimus*.

The present study describes (1) the presence of four-transmembrane domains and several *N*-glycosylation sites in sea urchin Syp based on the proteomic analysis of the sea urchin *Strongylocentrotus purpuratus* (Sp-Syp; PU_014316.3a, www.echinobase.org; *Cameron et al., 2009; Kudtarkar & Cameron, 2017*), (2) ontogenetic spatiotemporal expression patterns of Syp by anti-Sp-Syp antibody, (3) an ontogenetic analysis of GABA/Syp co-expression patterns along with, (4) the 3-MPA

PeerJ Preprints | https://doi.org/10.7287/peerj.preprints.26625v1 | CC BY 4.0 Open Access | rec: 6 Mar 2018, publ: 6 Mar 2018

92 treatment effect on the GABA/GAD expression patterns using three-dimensional
93 images of the CBAS by reconstructing whole-mount immunohistochemistry
94 (WMIHC) images obtained from confocal laser-scanning microscopy (CLSM).

95

96 **Materials and Methods**

97 Sea urchins (*H. pulcherrimus*, A. Agassiz) were collected near the Research Center for
98 Marine Biology, Tohoku University, Aomori, Japan and the Marine and Coastal
99 Research Center, Ochanomizu University, Chiba, Japan. Gametes were obtained by
100 intracoelomic injection of 0.5 M KCl. Eggs were inseminated and incubated in filtered
101 seawater (FSW) on a gyratory shaker or stirred gently with a propeller in an incubator at
102 15°C or 18°C until the appropriate developmental stages were reached. Larvae were fed
103 *Chaetoceros calcitrans* (Nisshin Marine Tech. Ltd, Yokohama, Japan) beginning at the
104 4-arm pluteus stage (4aPL) and continuing until various stages (described below) and
105 were incubated according to published methods (*Kiyomoto et al., 2014*).

106 *Antibody production*

107 Anti-Sp-GAD Ab was raised in rabbit using a synthetic peptide of Sp-GAD annotated
108 in the Genome Project of the sea urchin *S. purpuratus* (SPU_014316.3a),
109 (www.echinobase.org; *Cameron et al., 2009; Kudtarkar & Cameron, 2017*) which is a
110 sister species of *H. pulcherrimus*. The antigen peptide (^{598}FMLDEIERLGKPL^{610}) was
111 located near the C-terminal of the protein and was conjugated to a carrier protein
112 keyhole limpet hemocyanin (KLH) at the C-terminus of the protein ^{598}Phe via Cys
113 (Eurofin Genomics K.K. Tokyo). According to a homology search of the peptide
114 sequence by the NCBI Blast/Protein Sequence program
115 (https://blast.ncbi.nlm.nih.gov/Blast.cgi?PAGE=Proteins), no other sea urchin proteins
116 were included in the list of the search engine (*Altschul et al., 1997*;
117 https://blast.ncbi.nlm.nih.gov/Blast.cgi). Thus, the sequence was regarded to be
118 Sp-GAD-specific in sea urchin proteins.

119 Anti-Syp Ab was raised in rabbit using a synthetic peptide of Syp annotated in the
120 Genome Project of the sea urchin *S. purpuratus* (SPU_014316.3a)
121 (www.echinobase.org). The antigen peptide (^{241}KETTWFKQRME^{251}) was predicted to
122 be located near the C-terminus of the Syp protein on the interior surface of the EV
123 membrane (Fig. 1) and was conjugated to a carrier protein KLH at the C-terminus

PeerJ Preprints | https://doi.org/10.7287/peerj.preprints.26625v1 | CC BY 4.0 Open Access | rec: 6 Mar 2018, publ: 6 Mar 2018

^{241}Lys via Cys (Sigma-Aldrich Japan, Tokyo). According to a homology search of the peptide sequence by the NCBI Blast/Protein Sequence program (https://blast.ncbi.nlm.nih.gov/Blast.cgi?PAGE=Proteins), no other sea urchin proteins were included in the list of the search engine (*Altschul et al., 1997*; https://blast.ncbi.nlm.nih.gov/Blast.cgi). Thus, the sequence was regarded to be Sp-Syp-specific in sea urchin proteins.

Immunoblotting

Swimming (sBL) and mesenchyme blastulae (mBL), gastrulation half-completed gastrulae (1/2G), and prism larvae, 2aPL and 4aPL were dissolved in lysis buffer [10 mM Tris-HCl (pH 7.5) with 6 M urea and 1 % Nonidet P-40 (v/v)], lyophilized and stored at -20°C until use (*Katow et al., 2016*). These lyophilized samples were dissolved in 0.1 M Tris-SDS β-ME sample treatment buffer (Cosmo Bio Co., Ltd, Tokyo, 135-0016, Japan), loaded in gels (3 μg/lane) and separated on 2-15 % gradient sodium dodecyl sulfate-polyacrylamide gel [Multigel II Mini 2/15 (13W); Cosmo Bio., Ltd] electrophoresis with 3-color Prestained XL-Ladder molecular weight marker (APRO Life Science Inst. Inc., Naruto, Tokushima 771-0360, Japan). Gels were blotted to polyvinylidene difluoride membranes (Bio-Rad Laboratories, Inc. Hercules, CA 94547, USA), blocked with 5 % (w/v) skim milk diluted in Tris-buffered saline with 1 % Tween-20 (v/v) (TBST; Takara Bio Inc., Otsu, Shiga, 520-2193, Japan), and incubated with the anti-Syp Ab diluted at 1:1,000 for 2 h at ambient temperature (AmT). The primary Ab was detected by incubation with alkaline phosphatase (AP)-tagged goat anti-rabbit IgG Ab (AnaSpec, Inc. Fremont, CA 94555, USA) diluted 1:30,000 in TBST for 1 h at AmT, and visualized with the chromogenic reagents nitro-blue tetrazolium and 5-bromo-4-chloro-3′-indolyphosphate [BCIP/NBT Color Development Substrate, (Promega Co, Madison, WI 53711-5399, USA)] diluted in AP buffer (pH 9.5) according to the manufacturer's instructions.

Whole-mount immunohistochemistry (WMIHC)

Embryos and larvae were fixed in 4 % paraformaldehyde dissolved in filtered sea water (FSW) for 15 to 20 min at AmT. They were dehydrated through increasing concentrations of ethanol from 30 % to 70 % (v/v) and stored in 70 % ethanol at 4°C until use. Before onset of immunohistochemistry, the samples were hydrated in 0.1 M

PeerJ Preprints | https://doi.org/10.7287/peerj.preprints.26625v1 | CC BY 4.0 Open Access | rec: 6 Mar 2018, publ: 6 Mar 2018

phosphate buffered saline with 0.05 % Tween-20 (PBST; Medicago AB, Uppsala, Sweden).

Rabbit anti-GABA Ab (GeneTex Inc., Irvine, CA 92606, USA) was diluted at 1:150 in PBST and conjugated with the Zenon Alexa Fluor 488 rabbit IgG labeling kit (Thermo Fisher Scientific K.K., Yokohama, Japan) according to the manufacturer's protocol. Mouse anti-GABA Ab (Enzo Life Sciences, Inc., Farmingdale, NY 11735, USA) was diluted at 1:300 in PBST. Anti-Syp Ab was diluted at 1:1,000 in PBST. Anti-$GABA_AR$ Ab was raised in mouse (*Katow et al., 2013*) and diluted 1:500 in PBST. Anti-GAD Ab was diluted 1: 500 in PBST. These primary Abs were visualized by Alexa Fluor 488- or Alexa Fluor 594-tagged anti-mouse or rabbit IgG (diluted 1:500–750 in PBST; Invitrogen, Eugene, OR, USA) as described previously (*Katow et al., 2016*). The nuclei of the samples were further counterstained with 4', 6-diamidino-2-phenylindole (Sigma-Aldrich Co., St. Louis, MO 63103, USA) diluted at 0.1-0.5 μg/mL in PBST for 5 min at AmT. The specimens were examined under a Leica TCS SP8 CLSM (Leica Microsystems, Wetzlar, Germany). Images were analyzed with ImageJ 1.49v (NIH, Bethesda, MD, USA), and some of the images were rotated with Adobe Photoshop CSS Extended 12.0 X64 (Adobe Systems Inc., San Jose, CA, USA) for figure plates preparation.

3D reconstruction of CLSM optical cross sections of the CBAS

Forty-two 1 μm-thick optical sections of CLSM images from triple-stained 8aPL tissue sections of the CBAS were reconstructed in 3D using Amira 3D image processing software (FEI Visualization Sciences Group, Burlington, MA, USA) as described previously (*Katow et al., 2016*). The resultant optical Z-axis image was artificially and excessively elongated; thus, the 3D images did not correctly represent the original CLSM image. Therefore, the CBAS computer images were manually adjusted to 1/3 of the computed image size according to original images obtained by TEM (*Katow et al., 2016*). The 3D image was optically cross-sectioned at a 0.46 μm thickness perpendicular to the long axis of the CBAS to examine potential co-localization of the positive signals of GAD and GABA as described in the "Results".

3-MPA treatment

To examine the involvement of GAD in the CBAS in the process of GABA expression in the CB, GAD function was suppressed using 3-MPA (*Van der Heyden & Korf, 1978*).

PeerJ Preprints | https://doi.org/10.7287/peerj.preprints.26625v1 | CC BY 4.0 Open Access | rec: 6 Mar 2018, publ: 6 Mar 2018

Eight-arm plutei were incubated with 0.5 μM 3-MPA in FSW for 4 h at AmT to inhibit larval swimming activity (*Katow et al., 2013*). Control larvae were incubated without 3-MPA. After visual confirmation of inhibited swimming activity, the 3-MPA-treated larvae were fixed with 4 % paraformaldehyde diluted in FSW. The larvae were stained with mouse anti-GABA Ab and rabbit anti-Syp Ab and were examined under a CLSM as described above.

Results

Validation of anti-Sp-GAD Ab by Enzyme-Linked Immuno Sorbent Assay (ELISA) and WMIHC

The presently produced anti-Sp-GAD Ab binding to the antigen peptide was steadily detected up to 1:16,000 dilution, while preimmune serum barely detected the binding (Fig. 2A), indicating the peptide specificity of the Ab.

Using WMIHC, the Ab detected the CBAS of 6aPL (Fig. 2B). The binding pattern was consistent with our previous reports (*Katow et al., 2013; 2016*), which was conducted with a commercial anti-rat GAD ($GAD_{65/67}$) Ab. Contrarily, preimmune serum binding to the CBAS or any other larval feature was not detected (Fig. 2C), indicating the antigen specificity of the Ab.

Molecular property of Sp-Syp protein

Intercellular transmission of GABA involves SV that consists of synaptogyrin and Syp as a major membrane protein that is abundantly expressed in GABAergic neurons (*Abraham et al., 2011*). According to the EchinoBase (http://www.echinobase.org/Echinobase/ *Cameron et al., 2009; Kudtarkar & Cameron, 2017*), the sea urchin Syp (Sp-Syp; SPU_014316.3a) is comprised of 266 amino acids and is regarded as a likely ortholog of Syp (http://www.echinobase.org/Echinobase/Search/SpSearch/viewAnnoGeneInfo.php?spu_id=SPU_014316). According to *N*-glycosylation site analysis by the online database NetNGlyc 1.0 Server (Technical University of Denmark; http://www.cbs.dtu.dk/services/NetNGlyc/), four *N*-glycosylation sites at ^{103}NSTT^{106}, ^{113}NPSG^{116}, ^{193}NPTV^{196} and ^{219}NFSV^{222} were predicted (Fig. 1). However, NetNGlyc 1.0 Server predicted a low threshold potential for glycosylation at ^{113}NPSG^{116} (0.4502<0.5). Thus, *N*-glycosylation possibly occurs at the other three sites. Their potentials were above the threshold at 0.5850 (^{103}NSTT^{106}), 0.7291 (^{193}NPTV^{196}), and

PeerJ Preprints | https://doi.org/10.7287/peerj.preprints.26625v1 | CC BY 4.0 Open Access | rec: 6 Mar 2018, publ: 6 Mar 2018

0.6807 (^{219}NFSV^{222}). The NetNGlyc 1.0 Server also predicted the absence of signal peptide in Sp-Syp.

Using the open database TMHMM Server v. 2.0 (http://www.cbs.dtu.dk/services/TMHMM/) for prediction of transmembrane helices in proteins, an analysis of Sp-Syp predicted the presence of the MARVEL domain (https://www.ncbi.nlm.nih.gov/Structure/cdd/cddsrv.cgi?ascbin=8&maxaln=10&seltype=2&uid=322712), which is functionally involved in vesicular trafficking and membrane apposition (*Arthur and Stowell, 2007*). The domain is comprised of four transmembrane subdomains, which include ^{47}Gly-Thr^{69}, ^{120}Phe-Val^{142}, ^{155}Cys-Gly^{177} and ^{218}Leu-Ala^{240} (Fig. 3).

Validation of anti-Sp-Syp Ab by immunoblotting (IB) and WMIHC

In the GABAergic nervous system, GABA is encapsulated into EVs, including the endoplasmic reticulum and SV, before secretion to the adjacent target cells (*Aihara et al., 2001; Teng et al., 2013*). Syp is one of the major molecular markers of the SV (*Jahn et al., 1985; Wiedenmann et al., 1986*). To evaluate the potential involvement of Syp in GABA transmission in the GABAergic nervous system of the sea urchin larva that plays a major role in larval swimming activity (*Katow et al., 2013; 2016*), we analyzed GABA transmission and Syp involvement using immunochemical techniques.

The anti-Syp Ab bound to a single band at approximately 38 kDa in the prism larval lysate (Fig. 4A, lane 1), whereas preimmune rabbit serum did not (Fig. 4A, lane 2). The relative molecular mass (M_r) of the Ab-bound region was slightly larger than the theoretical value of 28.8 kDa that was calculated based on its amino acid sequence with Compute pI/Mw (ExPASy Compute pI/Mw tool, https://web.expasy.org/compute_pi/). This suggested the occurrence of post-translational modification, including glycosylation as described above.

Using WMIHC, anti-Syp Ab was detected on the 4aPL larval arms with a strand pattern of the CBAS (Fig. 4B), whereas preimmune serum did not bind to the pluteus (Fig. 4C). The IB and WMIHC data verified the immunospecificity of the anti-Syp Ab. A detailed examination of the WMIHC showed that the anti-Syp Ab bound to a strand of puncta (Fig. 4D, arrowheads) along the larval arm with several perikarya (Fig. 4D, arrows), which was consistent with our previous report on the CBAS (*Katow et al., 2016*).

Disturbed GABA expression by 3-MPA in larvae

PeerJ Preprints | https://doi.org/10.7287/peerj.preprints.26625v1 | CC BY 4.0 Open Access | rec: 6 Mar 2018, publ: 6 Mar 2018

Next, to examine the involvement of the GABA transmission mechanism in GABA expression in the CB, we analyzed the effect of 3-MPA on GABA expression and GAD distribution in the CB.

The triple-stained WMIHC of 8aPL with Abs against GABA, GAD, and nuclei detected the co-localization of GABA and GAD in the CBAS (Fig. 5A-1, -3), but GABA alone in the CB and the stomach (Fig. 5A-2, -3). Furthermore, the intensity of the GABA-positive signal in puncta of the CBAS at the anterior epaulet, which derives from the CB during the late pluteus stages (*Zamani, 2012*), was stronger than that in the CB (Fig. 5A-2, insets).

The punctate pattern in the CBAS that co-expressed GAD and GABA (Figs. 5G-3, H-3, Hh-3-1, Hh-3-2) or GAD and Syp (*Katow et al., 2016*) suggested the presence of GABA-enriched clumps of EVs in the CBAS. To ensure this possibility further, optical cross sections of the double-stained CBAS were reconstructed using Amira imaging software to produce 3D images as stated in the Methods. A 0.46 μm thick optical cross section of the CBAS was produced from the 3D image at the region indicated by a vertical dotted line (Fig. 5B). The optical cross section was produced from GAD/nuclei double-stained images (Fig. 5Bb-1) and GABA/nuclei double-stained images (Fig. 5Bb-2). These two images were then merged to examine the positional relationship between the GAD-positive and GABA-positive regions in the CBAS (Fig. 5Bb-3). The merged images suggested that GAD and GABA are co-localized at the puncta.

The WMIHC examination of the 3-MPA-treated larvae indicated that GAD expression was not affected by the inhibitor (Fig. 5C-1), while GABA expression declined significantly both in the CBAS and the CB (Fig. 5C-2, -3). Thus, the decline in GABA expression in the CB is not due to the inhibition of transmission activity but to the inhibition of GABA production, suggesting the involvement of vital GABA transmission process from puncta of the CBAS, suggesting the involvement of vital GABA transmission process from the puncta in the CBAS. In addition to these organs, the inhibitor decreased GABA immunoreactivity in the stomach (Fig. 5C-2).

Spatial analysis of $GABA_AR$ *and GAD expression in and near the CBAS*

The presence of the MARVEL domain in Sp-Syp suggests its involvement in the neurosecretory process (*Arthur & Stowell, 2007*). However, prior to studying Syp involvement in neurosecretory function in the sea urchin larva, we examined the immunohistochemical localization of the GABAergic system in the larval arms.

As above GAD/GABA double-stained WMIHC indicated (Fig. 5), GAD was intensely expressed in the CBAS, while GABA was slightly weakly detected.

PeerJ Preprints | https://doi.org/10.7287/peerj.preprints.26625v1 | CC BY 4.0 Open Access | rec: 6 Mar 2018, publ: 6 Mar 2018

Conversely, in the CB, GABA was detected almost uniformly, while GAD was not. This suggests the occurrence of a functional differentiation between the GABA producer and its receiver during development in the GABAergic nervous system in sea urchin larvae.

GABA binds to its receptor protein, $GABA_AR$, in the mammalian central nervous system after its synthesis (*Simeone et al., 2003*), which resembles our previous report that immunohistochemically suggests co-localization of GABA and $GABA_AR$ at the probable CB (*Katow et al., 2013*). The CBAS was not yet discovered then. The present WMIHC detected GAD in the CBAS but not in the CB (Fig. 6A, C). On the other hand, $GABA_AR$ was expressed in the CB but not in the CBAS (Fig. 6B, C). On the basis of the previous our report (*Katow et al., 2013*) and the present observations, it could be hypothesized that GABA synthesized by GAD in the CBAS is transmitted to the CB and captured by $GABA_AR$ that is expressed in there.

Spatiotemporal expression pattern of Syp during development

According to the IB analysis, Syp was not detected at the sBL stage (Fig. 7A, lane 1) but was distinctively detected beginning with and following the mBL stage until the 4aPL stage at a minimum (Fig. 7A, lane 2-6), excluding an interruption at the 1/2G stage (Fig. 7A, lane 3). At this stage, a faint positive signal was detected by increasing the loading amount of lysate from 3 μg to 4.5 μg (data not shown), which suggested that although the Syp-positive signal declined considerably, it was not entirely absent. At the later developmental period, the M_r of Syp increased by approximately 5.3±0.25 % (n=3) (4aPL) from 38.2±1.76 kDa (2aPL) (Fig. 7A, lane 5 and 6); however, the M_r did not change before or after the 1/2G stage (Fig. 7A, lane 2 to 5).

Consistent with the above IB observation, the WMIHC analysis detected no apparent Syp-positive signal in the sBL (Fig. 7B); however, small Syp-positive particles were seen in a small number of ectodermal cells in the mBL (Fig. 7C). At the 1/2G stage, a Syp-positive signal was faintly detected in the ectoderm (Fig. 7D). In contrast to these younger embryos, the prism larvae displayed an increased number of Syp-positive cells in the ectoderm (Fig. 7Ee-1, -2) and the blastocoel (Fig. 7Ff-1, -2). At the 2aPL stage, patches of Syp-positive cells were retained in the ectoderm (Fig. 7Gg-1), while the Syp-positive blastocoelar cells aligned to form fragmental strands on the basal side of the ectoderm (Fig. 7Gg-2). At the 4aPL stage, the Syp-positive strand appeared on the larval surface, particularly at the larval arms (arrows in Fig. 7H and Fig. 7Hh), which indicated that these larval surface strands are the CBAS (*Katow et al., 2016*). The Syp-positive CBAS was terminated at the left and right side of the upper oral region

PeerJ Preprints | https://doi.org/10.7287/peerj.preprints.26625v1 | CC BY 4.0 Open Access | rec: 6 Mar 2018, publ: 6 Mar 2018

(Fig. 7Hh, arrowheads in dotted box), indicating that the circumoral CBAS does not form a closed ring but forms an open ring at the periphery of the oral ectoderm. The short strand of the blastocoelar Syp-positive cells was prominent at the upper oral region (Fig. 7Hi, arrowhead). Thus, strand formation by the Syp-positive cells developed considerably beginning with and following the 2aPL stage, both on the larval body surface in the CBAS and in the blastocoel, which was consistent with a strong Syp-positive band detected by IB (Fig. 7A).

Comparative spatiotemporal expression pattern between GABA and Syp during development

Next, to examine the organization of Syp-expressing cells and the functional acquisition of GABAergic properties by the CBAS, the GABA/Syp expression pattern was analyzed by double-stained WMIHC during development.

Syp (Fig. 8A-1) and GABA (Fig. 8A-2) were not detected at the sBL stage (Fig. 8A-3). At the mBL stage, Syp-positive particles (Fig. 8B-1) were detected in the cytoplasm of the ectodermal cells in association with a weak GABA signal (Fig. 8B-2). Small cytoplasmic particles of Syp-positive signals were closely associated with GABA-positive signals, and both signals converged moderately well (Fig. 8B-3). At the 1/2G stage, a small number of ectodermal cells expressed Syp in the cytoplasm (Fig. 8C-1). The intensity of the immunoreaction of the Syp-positive cytoplasmic area was marginally stronger and regionally broader than that in younger embryos. Conversely, the GABA-positive signal was weaker than the Syp-positive signal (Fig. 8C-2). However, both positive signals appeared to converge at a similar cytoplasmic area (Fig. 8C-3).

In prism larvae, the number of Syp-expressing cells increased distinctively both in the ectoderm and the blastocoel (Fig. 8D-1, inset). GABA expression accompanied the increased Syp-positive signal and was detected more intensely than in the previous developmental stages in the ectoderm (Fig. 8D-2) and the blastocoelar cells (Fig. 8D-2, inset). However, these Syp and GABA signals were seemed not precisely co-localized (Fig. 8D-3, arrow in inset), suggesting that the Syp-positive sites were not completely shared with the GABA-positive sites.

At the 2aPL stage, while the body surface positive signals of Syp and GABA were not co-localized (Fig. 8E-1-E-3, arrowheads), both signals appeared to converge in the blastocoelar cells (Fig. 8E, Insets, arrow). At the 4aPL stage, the blastocoelar cells (Fig. 8F, small arrow) and the CBAS (Fig. 8F, arrow) appeared to co-express Syp and GABA

PeerJ Preprints | https://doi.org/10.7287/peerj.preprints.26625v1 | CC BY 4.0 Open Access | rec: 6 Mar 2018, publ: 6 Mar 2018

(Fig. 8F, arrow in insets). At the 6aPL stage, the Syp-positive signal in the CBAS and GABA-positive signal in the CB were intensified (Fig. 8G-2, G-3, arrowhead in Insets).

At the 8aPL stage, the Syp-positive signal was further intensified in the CBAS of the epaulettes (Fig. 8H-1, Hh-1-1, arrow) and the larval arms (Fig. 8H-1, Hh-1-2, arrows). The GABA-positive signal was also intensified in the CBAS (Fig. 8H-2, Hh-2-1, Hh-2-2, arrows) and the CB of the epaulettes (Fig. 8H-2, Hh-2-1, arrowhead) and the CBAS of the larval arms (Fig. 8H-2, Hh-2-2, arrows). However, both signals were not co-localized in the CB of the epaulettes (Fig. 8H-3, Hh-3-1), while in the CBAS of larval arm, both signals were co-localized (Fig. 8H-3, Hh-3-2).

Thus, GABA and Syp was not co-localized until the prism larva stage. Beginning with the 2aPL stage, the blastocoelar cells acquired co-localization of both signals. However, associated with the CBAS formation beginning with and following the 4aPL stage, the GABA and Syp expression sites converged in the CBAS, while the CB did not express Syp.

Discussion

Molecular properties of Sp-Syp

The higher apparent M_r of Sp-Syp (38 kDa) obtained by IB (Fig. 3A) compared to the M_r calculated from the number of amino acids (28.8 kDa) may be due to the presence of *N*-glycosylation sites, which affect the apparent M_r of Syp proteins by 12.4-21.4 % (*Wiedenmann, 1991*). The same context could be applicable for approximately 20% decline of M_r (approximately 30 kDa) at the 6aPL stage (*Katow et l., 2016*). Glycosylation is reported to be essential for Syp function (*Kwon & Chapman, 2011*). However, whether the slight increase of the M_r of Syp from the 2aPL stage to the 4aPL stage (Fig. 4A) has any causal relationship to functional modification has not been determined. Despite the prediction that Sp-Syp lacks a signal peptide sequence, *N*-glycosylation of the mammalian Syp has been reported for the tunicamycin digestion-induced decrease of the M_r of a Syp that also lacks a signal peptide (*Wiedenmann, 1991*). Thus, the predicted absence of the signal peptide sequence may not be important for *N*-glycosylation of Syp in general.

The isoelectric point of the Sp-Syp was predicted to be 5.69 (ExPASy Compute pI/Mw tool), which is slightly higher than that of the rat Syp (4.8-4.3; *Wiedenmann, 1991*). The present observation of a slight increase of the relative molecular mass of Syp at the 4aPL stage from the younger larvae (Fig. 4A) possibly involves a developmental stage-dependent glycosylation modification of the protein (*Scott & Panin 2014*).

PeerJ Preprints | https://doi.org/10.7287/peerj.preprints.26625v1 | CC BY 4.0 Open Access | rec: 6 Mar 2018, publ: 6 Mar 2018

However, its functional and developmental significance in the ontogeny of the CBAS and sea urchin larva remain to be elucidated.

The 194-amino acid MARVEL domain detected from ^{47}Gly to Ala^{240} in Sp-Syp (Fig. 1B) is consistent with known mammalian Syp as an archetypal member of the MARVEL-domain family (*Arthur & Stowell, 2007*), and further implicates Sp-Syp as an integral membrane protein. The domain also implicates Sp-Syp involvement in the SNARE-regulated fusion and recycling of SV (*Arhur & Stowell, 2007*). In cultured hippocampal neurons of E18 fetal rats, Syp is concentrated in puncta that correspond to presynaptic vesicle-filled varicosities (Fletcher *et al*., 1991), which are similar to the Syp-positive puncta in the CBAS (Fig. 6B) and suggest a neurosecretory role (Scarfone *et al*., 1991) of the CBAS in GABA transmission in the sea urchin larva.

The apparent co-localization of Syp-positive and GABA-positive signals at the puncta of the CBAS (Figs. 6H3, Hh-3-1, Hh-3-2) implicates the occurrence of GABA-enclosed puncta of SV and/or EV. Furthermore, the decrease of the GABA signal, both in the CBAS and the CB in the 3-MPA-treated larvae (Fig. 6C), strongly suggests GABA neurosecretion from the GAD-expressing CBAS to the CB. GABA in the CB is vital for maintaining larval swimming activity (*Katow et al., 2013*).

Although GABA is predominantly synaptic (*Vizi et al., 2010*), non-synaptic GABA secretion, as in crustaceans (*Pérez-Polanco et al., 2011*), may also occur in the CBAS. That possibility can be unraveled by Syp-knockdown or knockout studies. However, such studies proved to be unsuccessful due to redundant mechanisms of SV-associated neurosecretion, namely, compensation by synaptogyrin, which is an equally rich membrane protein in the SV (*Abraham et al., 2011*). Thus, an analysis using Syp/synaptogyrin double-knockout mice indicated a defect in SV endocytosis (*Spiwoks-Becker et al., 2001*), and such a study would likely be very informative for understanding GABA transmission mechanism in the sea urchin CBAS. However, no synaptogyrin gene has been identified in the *S. purpuratus* gene expression database (https://urchin.nidcr.nih.gov/blast/exp.html) to date; therefore, Syp/synaptogyrin double knockdown or knockout experiments may be inappropriate at present.

Spatiotemporal expression pattern of Syp during development

According to microarray analyses of Sp-Syp mRNA transcription activity, Sp-Syp mRNA transcription is initiated at 2 h post-fertilization (2-hpf, during the first cleavage period); however, that initiation period is followed by a period of low transcription activity that encompasses the blastula stages and the 1/2G stage. Nevertheless, at approximately 48-hpf (the late gastrula stage to the early prism stage), transcription

PeerJ Preprints | https://doi.org/10.7287/peerj.preprints.26625v1 | CC BY 4.0 Open Access | rec: 6 Mar 2018, publ: 6 Mar 2018

becomes high (*S. purpuratus* Genome Search, *S. purpuratus* Gene Expression; SPU_014316 Expression; https://urchin.nidcr.nih.gov/blast/exp.html). Although the mRNA and protein fluctuations are not well-correlated, due to the many factors involved in both processes, such as the degradation and transcription rates of mRNA compared to protein translation (*Vogel & Marcotte, 2012*), correlation between mRNA and protein levels has been proposed when the protein measurements are revised relative to the delay (*Gedeon & Bokes, 2012*). Accordingly, the apparently correlated temporal Syp mRNA and protein expression patterns closely resemble those seen in the Syp expression pattern of the rat spinal cord (*Bergmann et al., 1991*). Thus, the fluctuating immunochemical Syp protein expression pattern detected by IB at the 1/2G stage (Fig. 5A) may indicate correlation with Syp mRNA transcription, as shown by the microarray expression pattern described above. It also could be related to the maternal-to-zygotic transition (*Lee et al., 2014*) as has been reported RNA sedimentation pattern change from the pre-gastrula stages to the post-gastrulation stages during sea urchin development (*Nemer, 1963*). Further studies are yet to come.

Syp-expressing puncta formation has been reported in the boutons of GABAergic neurons in the cat thalamus (*Kultas-Ilinsky et al., 1985*) and the axons of vertebrates, including zebrafish (*Meyer & Smith, 2006*), rat (*Fletcher et al., 1991*), and mouse (*Harwell et al., 2016*), and invertebrates, such as *Octopus* (*Zhang et al., 2012*) and *Aplysia* (Jin *et al*. 2011). In the sea urchin embryos, the initial Syp-expressing cells are not morphologically differentiated nervous cells in terms of axonal projection formation and GABA expression (Fig. 5B-3). Rather, they are either patches of morphologically unspecified small numbers of ectodermal cells or similarly unspecified sparsely isolated blastocoelar cells. The number of Syp-expressing blastocoelar cells of the embryo is considerably smaller than those that do not express the protein (Fig. 7F). Thus, Syp expression may occur in a small subgroup of relatively unspecified ectodermal cells at the blastula stage and then ingress into the blastocoel to constitute a small subgroup of Syp-positive blastocoelar cells. The present WMIHC detected GABA expression in some of the blastocoelar cells beginning with and following the prism stage (Fig. 5D). This is apparently consistent with GAD-expressing cell formation before the CBAS forms during the later developmental stages (*Katow et al., 2014; Katow, 2015*) and suggests that Syp is expressed before the acquisition of neuronal morphological properties in these cells. This also seems to be consistent with the previous report on the ontogeny of Syp-expressing cell appearance in the central brain of *Drosophila* before the actual appearance of morphological neuronal cells (*Pech et al., 2015*) and that in the

PeerJ Preprints | https://doi.org/10.7287/peerj.preprints.26625v1 | CC BY 4.0 Open Access | rec: 6 Mar 2018, publ: 6 Mar 2018

neuroepithelium of the rat spinal cord (*Bergmann et al., 1991*). In this regard, the fundamental mechanism of Syp-expressing cell differentiation in the sea urchin may be shared with vertebrates and invertebrates. However, a further detailed cell lineage analysis remains to be conducted.

The resultant spatial segregation of GABA and Syp expression sites between the CB and the CBAS at the late pluteus stage appeared to be involved in the development-associated acquisition of the highly organized swimming regulation mechanism of larvae (*Mogami et al., 1991; Katow et al., 2013*).

Possible GABA signaling pathway from the CBAS to cilia in the CB

The GAD-expressing GABA synthetic site in the CBAS and the $GABA_AR$-expressing site in the CB are spatially segregated. The former also contains Syp/GABA-positive puncta and the latter expresses GABA accompanied by a $GABA_AR$-positive signal and GABA receptor-associated protein (GABARAP)-positive signal (*Katow et al., 2013*). Furthermore, GABA is detected near the basal body-specific γ-tubulin-expressing site (*Katow et al., 2013*). The localization of GABA near the basal body has been confirmed by immunoelectron microscopy in the rat oviduct (*Erdö et al., 1986*). In short, GABA, $GABA_AR$, and GABARAP are apparently co-localized at the basal body of the cilia in the CB, which implies that GABA is synthesized by GAD in the CBAS, packed into the Syp-expressing EV and transmitted to the CB cells. In these CB cells, GABA that was transmitted into the cytoplasm may bind to $GABA_AR$ that transfers the signal first to GABARAP, which is a microtubule-associated protein (MAP), and then to the basal body of the cilia (*Wang & Olsen, 2000*). Since GABARAP binds to tubulin at its N-terminus, the MAP is thought to connect $GABA_AR$ with the cytoskeleton (*Wang & Olsen, 2000*) in the GABA signal transmission pathway that promotes ciliary beating in the sea urchin larva. The proposed GABA signaling pathway is summarized in Figure 9.

CONCLUSIONS

Syp is expressed from the mBL stage until the onset of the metamorphosis. The period was interrupted around the 1/2G stage by declined Syp immunoreaction. At and after the pluteus stage, Syp was distinctively expressed at the GAD/GABA-positive puncta. In the CB, while GAD is not expressed, $GABA_AR$ and GABARAP are expressed closely to GABA-positive signal near the basal body of cilia. This suggests that Syp is

PeerJ Preprints | https://doi.org/10.7287/peerj.preprints.26625v1 | CC BY 4.0 Open Access | rec: 6 Mar 2018, publ: 6 Mar 2018

involved in GABA-enclosed EV formation in the CBAS, and that releases GABA to the CB.

Acknowledgements

This study was supported by the Aomori Foundation for Research, Art and Culture Promotion (No.147) to HK. This study was also partly supported by the Cooperative Research Project Program of the Joint Usage/ Research Center at the Institute of Development, Aging and Cancer, Tohoku University (No.34) to MK and HK.

Additional Information:

Competing Interests

The authors declare there are no competing interests.

Author Contributions

Hideki Katow conceived and designed the experiments, performed the experiments, analyzed the data, wrote paper, prepared figures.
Hiromi Yoshida performed 3D image reconstruction.
Masato Kiyomoto raised larvae for the experiments.
Tomoko Katow performed experiments, reviewed draft of the paper.

References

Abraham C, Bai L, Leube RE. 2011. Synaptogyrin-dependent modulation of synaptic neurotransmission in Caenorhabditis elegans. *Neuroscience* **190**: 75-88. DOI: 10.1016/j.neuroscience.2011.05.069.

Aihara Y, Inoue T, Tashiro T, Okamoto K, Komiya Y, Mikoshiba K. 2001. Movement of endoplasmic reticulum in the living axon is distinct from other membranous vesicles in its rate, form, and sensitivity to microtubule inhibitors. *Journal of Neuroscience Research* **65**: 236-246.

Altschul SF, Madden TL, Schäffer AA, Zhang J, Zhang Z, Miller W, Lipman DJ. 1997. Gapped BLAST and PSI-BLAST: a new generation of protein database search programs. *Nucleic Acids Research* **25**: 3389-3402.

Arthur CP, Stowell MHB. 2007. Structure of synaptophysin: A hexameric MARVEL-domain channel protein. *Structure* **15**: 707–714.

Bergmann M, Lahr G, Mayerhofer A, Gratzl M. 1991. Expression of synaptophysin during the prenatal development of the rat spinal cord: Correlation with basic differentiation processes of neurons. *Neuroscience* **42**: 569-582.

Calábria LK, Peixoto PMV, Lima ABP, Peixoto LG, de Moraes VRA, Teixeira RR, dos Santos CT, e Silva LO, da Silva MFR, dos Santos AAD, Garcia-Cairasco N, Martins AR, Espreafico EM, Espindola F.S. 2011. Myosins and DYNLL1/LC8 in the honey bee (*Apis mellifera* L.) brain. *Journal of Insect Physiology* **57**: 1300–1311.

Cameron RA, Samanta M, Yuan A, He D, Davidson E. 2009. SpBase: the sea urchin genome database and web site. *Nucleic Acids Research* **37**: D750-D754. DOI:10.1093/nar/gkn887

Erdö SL, Somogyi J, Hámori J, Amenta F. 1986. Light- and electron-microscopic visualization of gamma-aminobutyric acid and GABA-transaminase in the oviduct of rats. Predominant occurrence in epithelium. -*Cell and Tissue Research* **244**: 621-662.

Fletcher TL, Cameron P, De Camilli P, Banker G. 1991. The distribution of synapsin I and synaptophysin in hippocampal neurons developing in culture. *The Journal of Neuroscience* **11**: 1617-1626.

Gedeon T, Bokes P. 2012. Delayed protein synthesis reduces the correlation between mRNA and protein fluctuations. *Biophysical Journal* **103**: 377–385

Harwell CS, Coleman MP. 2016. Synaptophysin depletion and intraneuronal Aβ in organotypic hippocampal slice cultures from huAPP transgenic mice. *Molecular Neurodegeneration* **11**: 44 DOI: 10.1186/s13024-016-0110-7

568 **Jahn R, Schiebler W, Ouimet C, Greengard P. 1985.** A 38,000-dalton membrane
569 protein (p38) present in synaptic vesicles. *Proceedings of the National Academy of*
570 *Sciences of the United States of America* **82**:4131-4141.

571 **Jin I, Udo H, Hawkins RD. 2011.** Rapid increase in clusters of synaptophysin at onset
572 of homosynaptic potentiation in Aplysia. *Proceedings of the National Academy of*
573 *Sciences of the United States of America* **108**: 1656–1166.
574

575 **Katow H, Suyemitsu T, Ooka S, Yaguchi J, Jin-nai T, Kuwahara I, Katow T,**
576 **Yaguchi S, Abe H. 2010.** Development of a dopaminergic system in sea urchin
577 embryos and larvae. *Journal of Experimental Biology* **213**: 2808-2819.

578 **Katow H, Abe K, Katow T, Zamani A, Abe H. 2013.** Development of the
579 GABA-ergic signaling system and its role in larval swimming in the sea urchin.
580 *Journal of Experimental Biology* **216**: 1704-1716. DOI:10.1242/jeb.074856
581

582 **Katow H, Katow T, Abe K, Ooka S, Kiyomoto M, Hamanaka G. 2014.**
583 Mesomere-derived glutamate decarboxylase-expressing blastocoelar mesenchyme
584 cells of sea urchin larvae. *Biology Open* **3**: 94-102.
585

586 **Katow H. 2015.** Evolution and adaptation of tissue barriers: The quest for new models
587 and mechanisms of the epithelial-to-mesenchymal transition in sea urchin embryos.
588 *Tissue Barriers* **3**: 4, e1059004-1-23. DOI:10.1080/21688370.2015.1059004
589

590 **Katow H, Katow T, Yoshida H, Kiyomoto M, Uemura I. 2016.**
591 Immunohistochemical and ultrastructural properties of the ciliary band-associated
592 strand (CBAS) in sea urchin *Hemicentrotus pulcherrimus* larva. *Frontiers in Zoology*
593 **13**: 27 DOI: 10.1186/s12983-016-0159-8
594

595 **Kiyomoto M, Hamanaka G, Hirose M, Yamaguchi M. 2014.** Preserved echinoderm
596 gametes as a useful and ready-to-use bioassay material. *Marine Environmental*
597 *Research* **93**: 102-105. DOI: 10.1016/j.marenvres.2013.08.014.
598

599 **Kudtarkar P, Cameron RA. 2017.** Echinobase: an expanding resource for echinoderm
600 genomic information. *Database (Oxford)* **1**: 2017 DOI: 10.1093/database/bax074

Kultas-Ilinsky K. Ribak CE, Peterson GM, Oertel WH. 1985. A Description of the GABAergic neurons and axon terminals in the motor nuclei of the cat thalamus. *Journal of Neuroscience* **5**: 1346-1369.

Kwon SE, Chapman ER. 2011. Synaptophysin regulates the kinetics of synaptic vesicle endocytosis in central neurons. *Neuron* **9**: 847-854. DOI: 10.1016/j.neuron.2011.04.001.

Lee MT, Bonneau AR, Giraldez AJ., 2014. Zygotic genome activation during the maternal-to-zygotic transition. *Annual Review of Cell and Developmental Biology* **30**: 581–613. DOI:10.1146/annurev-cellbio-100913-013027.

McMahon HT, Bolshakov VY, Janz R, Hammer RE, Siegelbaum SA, Südhof TC.1996. Synaptophysin, a major synaptic vesicle protein, is not essential for neurotransmitter release. *Proceedings of the National Academy of Sciences of the United States of America* **93**: 4760–4764.

Nemer M. 1963. Old and new RNA in the embryogenesis of the purple sea urchin. *Proceedings of the National Academy of Sciences of the United States of America* **50**: 230-235.

Meyer MP, Smith SJ. 2006. Evidence from *In Vivo* Imaging That Synaptogenesis Guides the Growth and Branching of Axonal Arbors by Two Distinct Mechanisms. *Journal of Neuroscience* **26**: 3604 –3614.

Mogami Y, Fujima K, Baba SA. 1991. Five different states of ciliary activity in the epaulette of echinoplutei. *Journal of Experimental Biology* **155**: 65-75.

Pech U, Revelo NH, Seitz KJ, Rizzoli SO, Fiala A. 2015. Optical dissection of experience-dependent pre- and postsynaptic plasticity in the *Drosophila* brain. *Cell Reports* **10**: 2083–2095.

Pérez-Polanco P, Garduño J, Cebada J, Zarco N, Segovia J, Lamas M, García U. 2011. GABA and GAD expression in the X-organ sinus gland system of the *Procambarus clarkii* crayfish: inhibition mediated by GABA between X-organ neurons. *Journal of Comparative Physiology. A, Neuroethology, Sensory, Neural, and Behavioral Physiology* **197**: 923-938. DOI: 10.1007/s00359-011-0653-6.

PeerJ Preprints | https://doi.org/10.7287/peerj.preprints.26625v1 | CC BY 4.0 Open Access | rec: 6 Mar 2018, publ: 6 Mar 2018

Rabelo ÉML, Franco GR, Azevedo VCA, Pena HB, Santos TM, Meira WSF, Rodrigues NA, Ortega JM, Pena ADJ. 1997. Update of the gene discovery program in *Schistosoma mansoni* with the expressed sequence Tag approach. *The Memórias do Instituto Oswaldo Cruz* **92**: 625-629.

Scarfone E, Demêmes D, Sans A. 1991. Synapsin I and Synaptophysin Expression during Ontogenesis of the. Mouse Peripheral Vestibular System. *Journal of Neuroscience* **11**: 1173-1181.

Scott, H., and Panin, V. M. 2014. N-glycosylation in Regulation of the Nervous System. *The Advances in Neurobiology* **9**: 367–394. DOI:10.1007/978-1-4939-1154-7_17.

Sethi M, Mishra S, Kaul JM, Vasudeva N. 2013. Morphogenesis and maturation of synapses in developing human cochlear ganglion. *Journal of Morphological Science* **30**: 289-298.

Simeone TA, Donevan SD, Rho JM. 2003. Molecular Biology and Ontogeny of γ-Aminobutyric Acid (GABA) Receptors in the Mammalian Central Nervous System. *Journal of Child Neurology* **18**: 39 DOI:10.1177/08830738030180012101

Soliman S. 1983. Pharmacological control of ciliary activity in the young sea urchin larva. Effects of monoaminergic agents. *Comparative Biochemistry and Physiology - Part C: Toxicology & Pharmacology* **767**: 181-191.

Spiwoks-Becker I, Vollrath L, Seeliger MW, Jaissle G, Eshkind LG, Leube RE. 2001. Synaptic vesicle alterations in rod photo- receptors of synaptophysin-deficient mice. *Neuroscience* **107**: 127– 142.

Stevens RJ, Akbergenova Y, Jorquer RA, Littleton JT. 2012. Abnormal Synaptic Vesicle Biogenesis in *Drosophila Synaptogyrin* Mutants. *Journal of Neuroscience* **32**: 18054–18067. DOI:10.1523/JNEUROSCI.2668-12.2012.

Strathman RR, Grünbaum D. 2006. Good eaters, poor swimmers: compromises in larval form. *Integrative and Comparative Biology* **46**: 312-322. DOI: 10.1093/icb/icj031.

PeerJ Preprints | https://doi.org/10.7287/peerj.preprints.26625v1 | CC BY 4.0 Open Access | rec: 6 Mar 2018, publ: 6 Mar 2018

Teng L, Tang Y-B, Sun F, An S-M, Zhang C, Yang X-J, Lv H-Y, Lu Q, Cui Y-Y, Hu J-J, Zhu L, Chen H-Z. 2013. Non-Neuronal Release of Gamma-Aminobutyric Acid by Embryonic Pluripotent Stem Cells. *Stem Cells and Development* **22**: 2944-2953. DOI: 10.1089/scd.2013.0243

Van der Heyden JAM, Korf J. 1978. Regional levels of GABA in the brain: rapid semiautomated assay and prevention of postmortem increase by 3-mercapto-propionic acid. *Journal of Neurochemistry* **31**: 197-203.

Vizi ES, Fekete A, Karoly R, Mike A. 2010. Non-synaptic receptors and transporters involved in brain functions and targets of drug treatment. *British Journal of Pharamacology* **160**: 785-809. DOI:10.1111/j.1476-5381.2009.00624.x

Vogel C, Marcotte EM. 2012. Insights into the regulation of protein abundance from proteomic and transcriptomic analyses. *Nature Review Genetics* **13**: 227–232. DOI:10.1038/nrg3185.

Wang H, Olsen RW. 2000. Binding of the GABA(A) receptor-associated protein (GABARAP) to microtubules and microfilaments suggests involvement of the cytoskeleton in GABARAP-$GABA_A$ receptor interaction. *Journal of Neurochemistry* **275**: 644-655.

Wiedenmann B, Franke WW, Kuhn C, Moll R, Gould VE. 1986. Synaptophysin: a marker protein for neuroendocrine cells and neoplasms. *Proceedings of the National Academy of Sciences of the United States of America* **83**: 3500-3504.

Wiedenmann B. 1991. Synaptophysin: A widespread constituent of small neuroendocrine vesicles and a new tool in tumor diagnosis. *Acta Oncologica* **30**: 435-440. DOI: 10.3109/02841869109092398

Yaguchi S, Kanoh K, Amemiya S, Katow H. 2000. Initial analysis of immunochemical cell surface properties, location and formation of the serotonergic apical ganglion in sea urchin embryos. *Development Growth & Differentiation* **42**: 479-488.

PeerJ Preprints | https://doi.org/10.7287/peerj.preprints.26625v1 | CC BY 4.0 Open Access | rec: 6 Mar 2018, publ: 6 Mar 2018

Yaguchi S, Katow H. 2003. Expression of Tryptophan 5-Hydroxylase Gene during Sea Urchin Neurogenesis and Role of Serotonergic Nervous System in Larval Behavior. *Journal of Comparative Neurology* **466**: 219-229.

Zamani A. 2012. Role of cytokinetic factors in the formation of epaulets, a set of ciliary bands in the trunk region, during late pluteus stages in sea urchin. Master of Life Sciences Thesis, Tohoku University. B1BM2601.

Zhang X, Mao Y, Huang Z, Qu M, Chen J, Ding S, Hong J, Sun T. 2012. Transcriptome analysis of the *Octopus vulgaris* central nervous system. -*PLoS ONE* **7**: e40320. DOI:10.1371/journal.pone.0040320

709 **Figure Legends**
710
711 **Fig. 1.** Primary structure of Sp-Syp protein and *N*-glycosylation sites (red letters). Blue
712 letters; lower possibility of *N*-glycosylation. Blue box; antigen peptide region, Red
713 letter; *N*-glycosylation sites.
714
715 **Fig. 2. Anti-Sp-GAD antibody (Ab) validation. (A)** ELISA assay. The antibody titer
716 is predicted to be sufficient until 1:16,000 dilution. Preimmune serum binding to the
717 peptide is negligible throughout the all dilution ratios tested. (**B**) Whole-mount
718 immunohistochemistry shows anti-Sp-GAD Ab binding at the ciliary band-associated
719 strand (green) of 6-arm pluteus larva. (**C**) WMIHC of preimmune serum shows no
720 positive signal throughout the larval body of 6-arm pluteus. Scale bars, 100 μm.
721
722 **Fig. 3. Secondary structures of Sp-Syp protein.** Predicted four-transmembrane
723 domain helices (TM, red bars). Blue box near the C-terminus; antigen peptide location.
724 Inside, Inside the endoplasmic vesicle. Outside, Cytoplasmic region.
725
726 **Fig. 4. Anti-Sp-Syp antibody validation. (A)** Immunoblotting of a 4-arm plutei (4aPL)
727 lysate by anti-Sp-Syp antibody (Ab) detected a band at approximately 38 kDa (lane 1,
728 arrow), whereas preimmune serum was negative (lane 2). **(B)** Whole-mount
729 immunohistochemistry of a 4aPL by the Ab detected strand features at the larval arms
730 (arrow) and in the blastocoel (arrowheads). (**C**) Preimmune serum applied to a 6aPL
731 was negative. (**D**) Higher magnification of the post-oral arms of the antibody applied to
732 a 4aPL indicates anti-Syp Ab-positive puncta at a single strand along the larval arms
733 (arrowheads) with four perikarya (arrows). Scale bars, 75 μm (B), 100 μm (C) and 25
734 μm (D).
735
736 **Fig. 5. Decreased expression of GABA in the ciliary band (CB) and the ciliary**
737 **band-associated strand (CBAS) in a 3-MPA-treated 8-arm pluteus (8aPL)**
738 **triple-stained for GAD (green), GABA (red) and nuclei (blue).** (**A**) Left side view of
739 a control 8aPL. GAD-positive signal was detected in the CBAS of the larval arms,
740 including the epaulette (dotted box) (A-1). The CBAS is also GABA-positive (A-2,
741 A-3). Insets, higher magnification of the epaulette shown by a dotted box in the main
742 frame. Arrow, the CBAS. Vertical line, the CB region. (**B**) 3D reconstruction image of
743 the triple-stained epaulette region shown by insets of (A). Vertical line, the CB region.
744 (**Bb-1~Bb-3**) 0.46 μm-thick optical cross-section of the 3D reconstructed CBAS at the

PeerJ Preprints | https://doi.org/10.7287/peerj.preprints.26625v1 | CC BY 4.0 Open Access | rec: 6 Mar 2018, publ: 6 Mar 2018

745 dotted line (b) in (B). (b-1) GAD/nuclei stained image. (b-2) GABA/nuclei stained
746 image. (b-3) Merged image between (b-1) and (b-2). (**C**) a 3-MPA-treated 8aPL. (C-1),
747 GAD/nuclei double-stained. (C-2), GABA/nuclei double-stained. (C-3), merged image
748 between (C-1) and (C-2). Insets, higher magnification of the epaulette shown by a
749 dotted box in the main frame. Arrow, CBAS. Arrowhead, CB. Stm, stomach. Scale bars,
750 100 μm (A-1, C-1), 10 μm (A, inset, B), 20 μm (C-1, inset).
751
752 **Fig. 6. Oral view of an 8aPL showing GAD (red)-expressing CBAS and $GABA_AR$**
753 **(green)-expressing CB at the epaulette. (A)** GAD/nuclei double-stained image. (**B**)
754 $GABA_AR$/nuclei double-stained image of the same area as (A). (**C**) Merged image
755 between (A) and (B). Bottom row images are a higher magnification of the box in the
756 main frame. Arrows, the CBAS. Arrowheads, the CB. Scale bars, 100 μm (A) and 25
757 μm [inset of (A)].
758
759 **Fig. 7. Spatiotemporal Syp expression pattern by immunoblotting (A) and**
760 **whole-mount immunohistochemistry (B-H).** (**A**) Sequential expression pattern of the
761 anti-Syp antibody-positive band from the mesenchyme blastula stage (lane 2, mBL),
762 through the prism larval stage (lane 4, Prism), a 2-arm pluteus stage (lane 5, 2aPL), and
763 a 4-arm pluteus stage (lane 6, 4aPL), but not at the swimming blastula stage (lane 1,
764 sBL) and 1/2G stage (lane 3). (**B**) Swimming blastula. Syp-positive signal was not
765 detected. (**C**) Mesenchyme blastula. Inset, higher magnification image at the box of the
766 main frame showing small Syp-positive particles near the nuclei. (**D**) 1/2G. Smeared
767 faint Syp-positive cytoplasmic signal was detected. Inset, higher magnification image of
768 the box in the main frame. (**E**) Surface view of the left side of a prism larva. Inset (e-1),
769 higher magnification of the box (e-1) in the main frame. Two ectodermal cells indicate
770 weak positive signal near the nuclei. Inset (e-2), higher magnification of the box (e-2) in
771 the main frame. Four ectodermal cells indicate strong positive signal around the nucleus.
772 (**F**) Optical cross section of the (E) Syp-positive coelomic cells near the archenteron (ar).
773 Inset (f-1, f-2), higher magnification of blastocoelar cells with strong cytoplasmic
774 Syp-positive signal. (**G**) Oral view of a 2aPL. Inset (g-1), Syp-positive ectodermal cells.
775 Inset (g-2), Syp-positive blastocoelar cells. Insets are higher magnification of the cells
776 shown by the boxes in the main frame. (**H**) Oral view of a 4aPL. Arrow, the ciliary
777 band-associated strand (CBAS) on the larval arms. Arrowhead, blastocoelar
778 Syp-positive cell strand. mo, larval mouth. Inset (h), higher magnification of the box (h)
779 in the main frame shows the CBAS with perikarya (arrows). Arrowheads, left and right
780 terminals of the CBAS. Inset (i), 24 μm inside of the blastocoel of the oral lobe shown

PeerJ Preprints | https://doi.org/10.7287/peerj.preprints.26625v1 | CC BY 4.0 Open Access | rec: 6 Mar 2018, publ: 6 Mar 2018

by a box in (h). Arrowhead, Syp-positive blastocoelar cells. Scale bars, 25 μm (B, D), 50 μm (E, F, G), 100 μm (H).

Fig. 8. Spatiotemporal expression gap between Syp (green) and GABA (red) during development. (**A**) Swimming blastula (sBL). Syp and GABA were not detected. (**B**) Mesenchyme blastula (mBL). Small cytoplasmic Syp-positive particles (B-1) were accompanied by a faint GABA-positive area (B-2, B-3). Insets, higher magnification images of the box in the main frame. (**C**) Gastrulation half-completed gastrula (1/2G). Syp-positive cytoplasmic signal spread broader than in the mBL (C-1), which was accompanied by smeared GABA-positive area (C-2, C-3). Insets, higher magnification images of the box in the main frame. Arrow in insets, GABA-positive signal near Syp-positive area. (**D**) Optical cross section of a prism larva showing blastocoelar cells near the blastopore (Bp). Syp-positive signal in an ectodermal cell was evident in the cytoplasm (D-1), which was accompanied by GABA-positive signal (D-2, D-3). Inset, higher magnification of the area shown by the main frame. Arrow in insets, GABA-positive signal was accompanied by Syp-positive signal. (**E**) Oral view of an early 2-arm pluteus (2aPL). Positive signals of GABA and Syp in an ectodermal cell were not co-localized (arrowheads), while in the fragmental strand of blastocoelar cells these two positive signals were co-localized (arrow in Inset of E-1 for Syp, Insets of E-2 for GABA, and E-3 for merged image). Inset, higher magnification image of optical cross section showing blastocoelar cell strands at the area shown by the box in the main frame. (**F**) Oral view of a 4-arm pluteus (4aPL). Arrow, postoral ciliary band-associated strand (CBAS). Small arrow, blastocoelar cells. Arrowhead, GABA-positive stomach. Insets, higher magnification of the post-oral CBAS shown by the boxes in the main frames. Arrows, CBAS. Arrowheads, ciliary band (CB). (**G**) Oral view of a 6-arm pluteus (6aPL). Arrows, CBAS. Asterisks, Syp-positive blastocoelar cells. Insets, higher magnification of the epaulet shown by the boxes in the main frame. Arrow, CBAS. Arrowhead, CB. (**H**) Aboral view of an 8-arm pluteus (8aPL). Inset (h-1-1) to (h-3-2), higher magnification of epaulet (h-1-1, h-2-1, and h-3-1) and posterodorsal arm (h-1-2, h-2-2, and h-3-2) indicated by the boxes in the main frame. Arrows, CBAS. Arrowheads, CB. Stm, stomach. Scale bars, 25 μm (A-E), 5 μm (D-1 inset), 100 μm (F, G), 200 μm (H).

Fig. 9. Summary of predicted GABAergic signal transmission pathway to the ciliary band and cilia. The present and previous studies suggest the contribution of

PeerJ Preprints | https://doi.org/10.7287/peerj.preprints.26625v1 | CC BY 4.0 Open Access | rec: 6 Mar 2018, publ: 6 Mar 2018

GAD in the ciliary band-associated strand (CBAS) to larval swimming through transmission of GABA via synaptophysin-containing endoplasmic vesicles (EV) to the ciliary band cells. Then, GABA transmitted to the cytoplasm of the CB cells binds to $GABA_AR$ near the basal body, and then, $GABA_AR$ transmits the signal to GABARAP and tubulin in the cilia of the basal body.

PeerJ Preprints | https://doi.org/10.7287/peerj.preprints.26625v1 | CC BY 4.0 Open Access | rec: 6 Mar 2018, publ: 6 Mar 2018

Figure 1(on next page)

Primary structure of Sp-Syp protein and N-glycosylation sites.

Blue letters; lower possibility of N-glycosylation. Blue box; antigen peptide region, Red letter; N-glycosylation sites.

Fig. 1. Katow et al

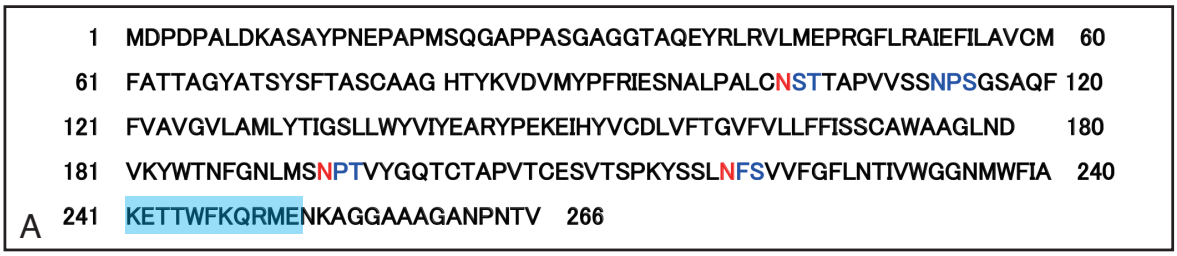

Figure 2(on next page)

Anti-Sp-GAD antibody (Ab) validation.

(A) ELISA assay. The antibody titer is predicted to be sufficient until 1:16,000 dilution. Preimmune serum binding to the peptide is negligible throughout the all dilution ratios tested. (B) Whole-mount immunohistochemistry shows anti-Sp-GAD Ab binding at the ciliary band-associated strand (green) of 6-arm pluteus larva. (C) WMIHC of preimmune serum shows no positive signal throughout the larval body of 6-arm pluteus. Scale bars, 100 µm.

Fig. 2. Katow et al.

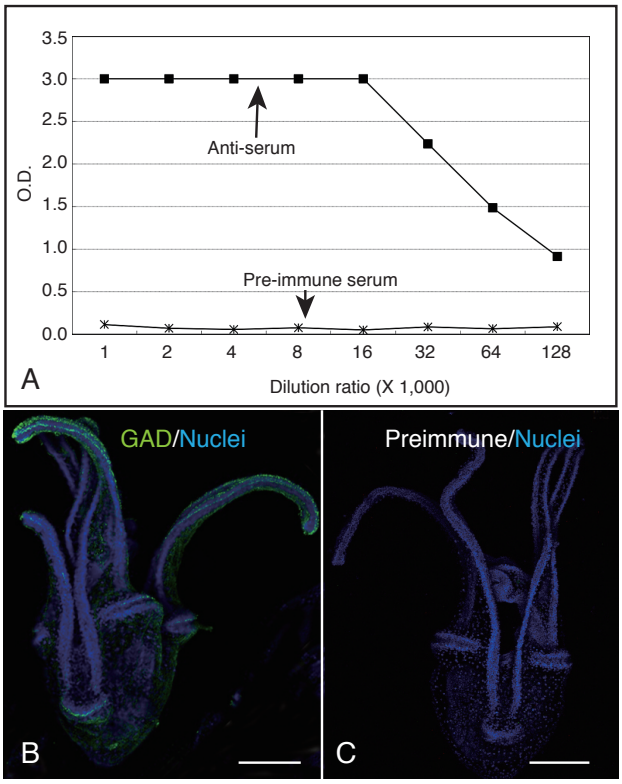

Figure 3(on next page)

Secondary structures of Sp-Syp protein.

Predicted four-transmembrane domain helices (TM, red bars). Blue box near the C-terminus; antigen peptide location. Inside, Inside the endoplasmic vesicle. Outside, Cytoplasmic region.

Fig. 3. Katow et al.

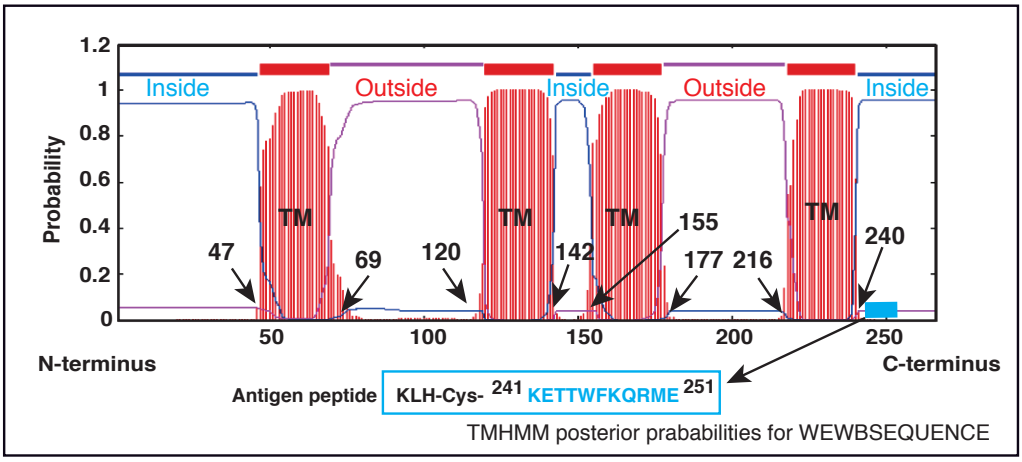

Figure 4(on next page)

Anti-Sp-Syp antibody validation.

(A) Immunoblotting of a 4-arm plutei (4aPL) lysate by anti-Sp-Syp antibody (Ab) detected a band at approximately 38 kDa (lane 1, arrow), whereas preimmune serum was negative (lane 2). (B) Whole-mount immunohistochemistry of a 4aPL by the Ab detected strand features at the larval arms (arrow) and in the blastocoel (arrowheads). (C) Preimmune serum applied to a 6aPL was negative. (D) Higher magnification of the post-oral arms of the antibody applied to a 4aPL indicates anti-Syp Ab-positive puncta at a single strand along the larval arms (arrowheads) with four perikarya (arrows). Scale bars, 75 µm (B), 100 µm (C) and 25 µm (D).

Fig. 4. Katow et al

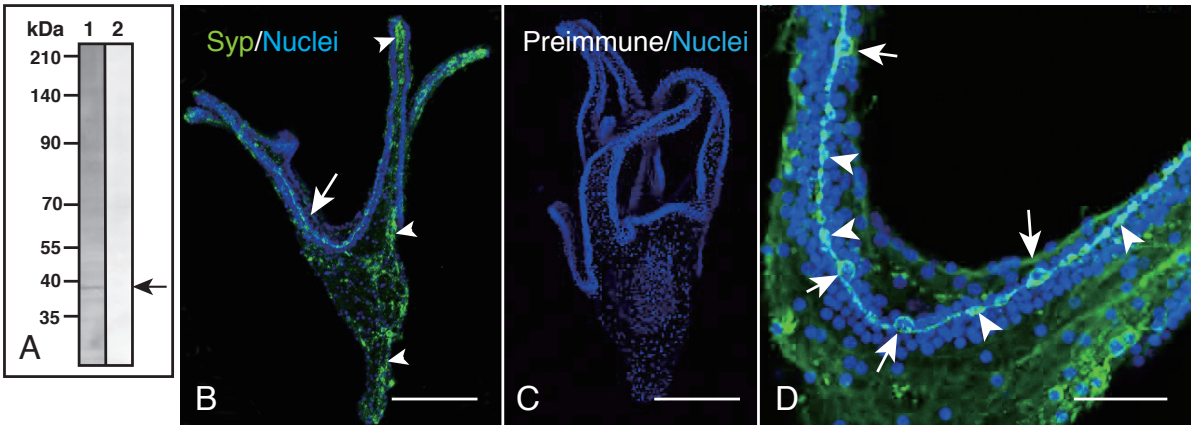

Figure 5(on next page)

Decreased expression of GABA in a 3-MPA-treated 8-arm pluteus.

(A) Left side view of a control 8aPL. GAD-positive signal was detected in the CBAS of the larval arms, including the epaulette (dotted box) (A-1). The CBAS is also GABA-positive (A-2, A-3). Insets, higher magnification of the epaulette shown by a dotted box in the main frame. Arrow, the CBAS. Vertical line, the CB region. (B) 3D reconstruction image of the triple-stained epaulette region shown by insets of (A). Vertical line, the CB region. (Bb-1~Bb-3) 0.46 µm-thick optical cross-section of the 3D reconstructed CBAS at the dotted line (b) in (B). (b-1) GAD/nuclei stained image. (b-2) GABA/nuclei stained image. (b-3) Merged image between (b-1) and (b-2). (C) a 3-MPA-treated 8aPL. (C-1), GAD/nuclei double-stained. (C-2), GABA/nuclei double-stained. (C-3), merged image between (C-1) and (C-2). Insets, higher magnification of the epaulette shown by a dotted box in the main frame. Arrow, CBAS. Arrowhead, CB. Stm, stomach. Scale bars, 100 µm (A-1, C-1), 10 µm (A, inset, B), 20 µm (C-1, inset).

Fig. 5. Katow et al

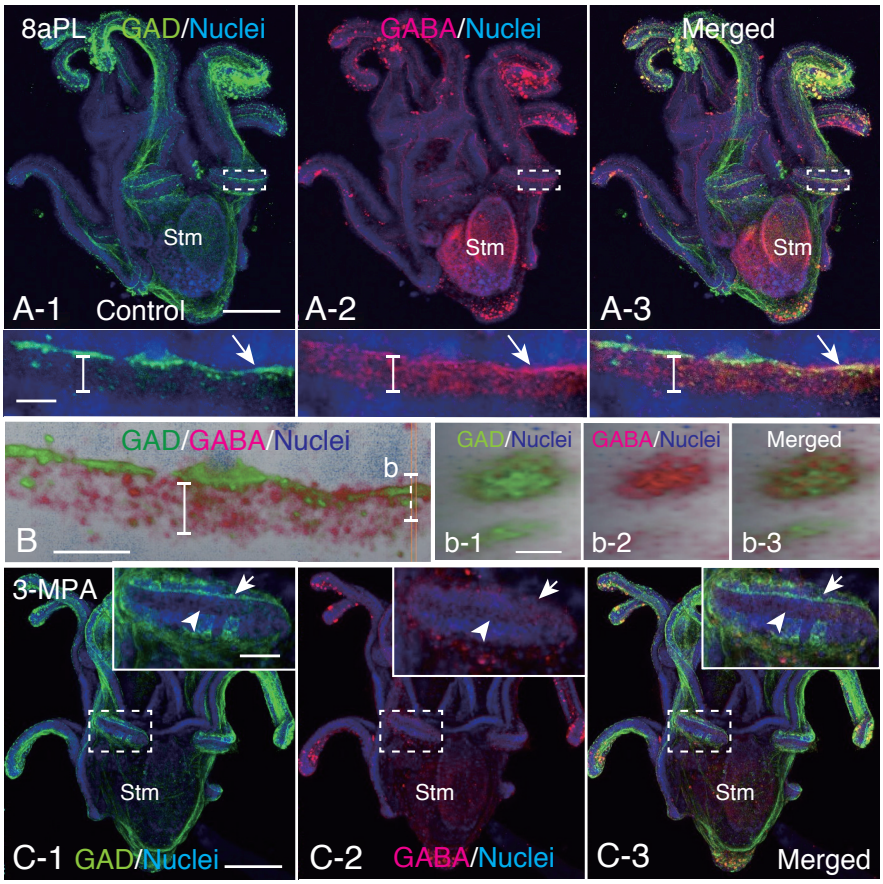

Figure 6(on next page)

An 8aPL showing GAD-expressing CBAS and GABAAR-expressing CB.

(A) GAD/nuclei double-stained image. (B) GABAAR/nuclei double-stained image of the same area as (A). (C) Merged image between (A) and (B). Bottom row images are a higher magnification of the box in the main frame. Arrows, the CBAS. Arrowheads, the CB. Scale bars, 100 μm (A) and 25 μm [inset of (A)].

Fig. 6. Katow et al.

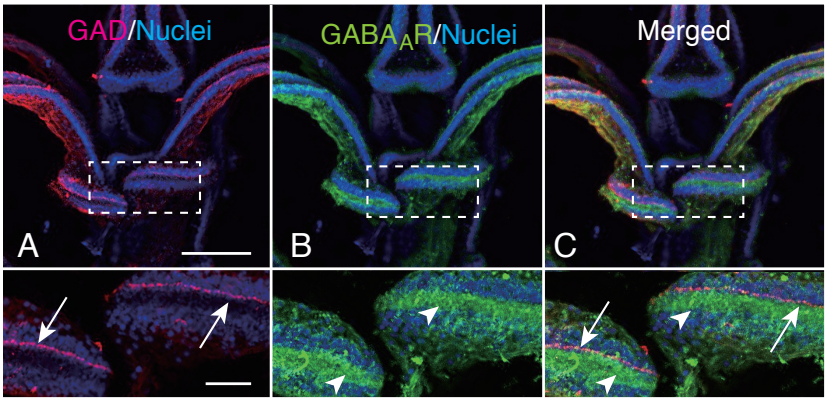

Figure 7 (on next page)

Spatiotemporal Syp expression pattern.

(A) Sequential expression pattern of the anti-Syp antibody-positive band from the mesenchyme blastula stage (lane 2, mBL), through the prism larval stage (lane 4, Prism), a 2-arm pluteus stage (lane 5, 2aPL), and a 4-arm pluteus stage (lane 6, 4aPL), but not at the swimming blastula stage (lane 1, sBL) and 1/2G stage (lane 3). (B) Swimming blastula. Syp-positive signal was not detected. (C) Mesenchyme blastula. Inset, higher magnification image at the box of the main frame showing small Syp-positive particles near the nuclei. (D) 1/2G. Smeared faint Syp-positive cytoplasmic signal was detected. Inset, higher magnification image of the box in the main frame. (E) Surface view of the left side of a prism larva. Inset (e-1), higher magnification of the box (e-1) in the main frame. Two ectodermal cells indicate weak positive signal near the nuclei. Inset (e-2), higher magnification of the box (e-2) in the main frame. Four ectodermal cells indicate strong positive signal around the nucleus. (F) Optical cross section of the (E) Syp-positive coelomic cells near the archenteron (ar). Inset (f-1, f-2), higher magnification of blastocoelar cells with strong cytoplasmic Syp-positive signal. (G) Oral view of a 2aPL. Inset (g-1), Syp-positive ectodermal cells. Inset (g-2), Syp-positive blastocoelar cells. Insets are higher magnification of the cells shown by the boxes in the main frame. (H) Oral view of a 4aPL. Arrow, the ciliary band-associated strand (CBAS) on the larval arms. Arrowhead, blastocoelar Syp-positive cell strand. mo, larval mouth. Inset (h), higher magnification of the box (h) in the main frame shows the CBAS with perikarya (arrows). Arrowheads, left and right terminals of the CBAS. Inset (i), 24 µm inside of the blastocoel of the oral lobe shown by a box in (h). Arrowhead, Syp-positive blastocoelar cells. Scale bars, 25 µm (B, D), 50 µm (E, F, G), 100 µm (H).

Fig. 7. Katow et al.

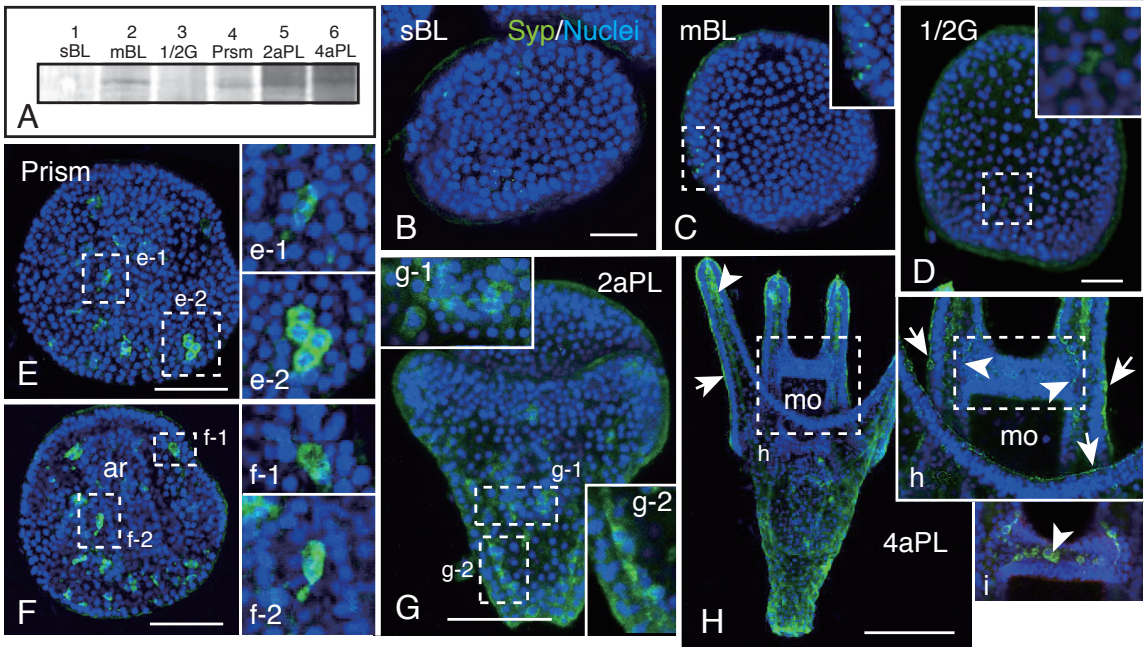

Figure 8

Spatiotemporal expression gap between Syp and GABA.

(A) Swimming blastula (sBL). Syp and GABA were not detected. (B) Mesenchyme blastula (mBL). Small cytoplasmic Syp-positive particles (B-1) were accompanied by a faint GABA-positive area (B-2, B-3). Insets, higher magnification images of the box in the main frame. (C) Gastrulation half-completed gastrula (1/2G). Syp-positive cytoplasmic signal spread broader than in the mBL (C-1), which was accompanied by smeared GABA-positive area (C-2, C-3). Insets, higher magnification images of the box in the main frame. Arrow in insets, GABA-positive signal near Syp-positive area. (D) Optical cross section of a prism larva showing blastocoelar cells near the blastopore (Bp). Syp-positive signal in an ectodermal cell was evident in the cytoplasm (D-1), which was accompanied by GABA-positive signal (D-2, D-3). Inset, higher magnification of the area shown by the main frame. Arrow in insets, GABA-positive signal was accompanied by Syp-positive signal. (E) Oral view of an early 2-arm pluteus (2aPL). Positive signals of GABA and Syp in an ectodermal cell were not co-localized (arrowheads), while in the fragmental strand of blastocoelar cells these two positive signals were co-localized (arrow in Inset of E-1 for Syp, Insets of E-2 for GABA, and E-3 for merged image). Inset, higher magnification image of optical cross section showing blastocoelar cell strands at the area shown by the box in the main frame. (F) Oral view of a 4-arm pluteus (4aPL). Arrow, postoral ciliary band-associated strand (CBAS). Small arrow, blastocoelar cells. Arrowhead, GABA-positive stomach. Insets, higher magnification of the post-oral CBAS shown by the boxes in the main frames. Arrows, CBAS. Arrowheads, ciliary band (CB). (G) Oral view of a 6-arm pluteus (6aPL). Arrows, CBAS. Asterisks, Syp-positive blastocoelar cells. Insets, higher magnification of the epaulet shown by the boxes in the main frame. Arrow, CBAS. Arrowhead, CB. (H) Aboral view of an 8-arm pluteus (8aPL). Inset (h-1-1) to (h-3-2), higher magnification of epaulet (h-1-1, h-2-1, and h-3-1) and posterodorsal arm (h-1-2, h-2-2, and h-3-2) indicated by the boxes in the main frame. Arrows, CBAS. Arrowheads, CB. Stm, stomach.

Scale bars, 25 μm (A-E), 5 μm (D-1 inset), 100 μm (F, G), 200 μm (H).

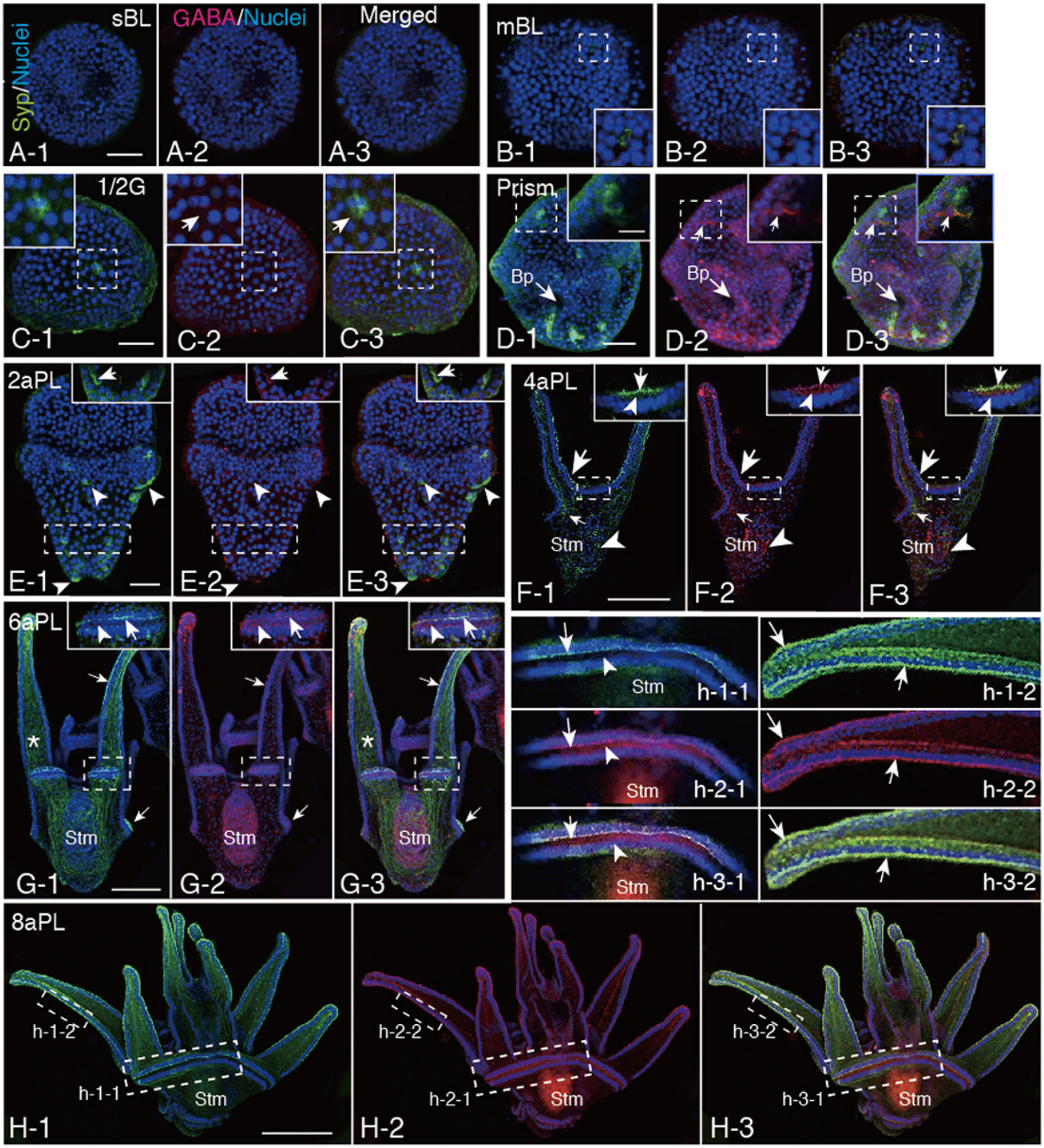

Figure 9

Summary of predicted GABAergic signal transmission pathway.

The present and previous studies suggest the contribution of GAD in the ciliary band-associated strand (CBAS) to larval swimming through transmission of GABA via synaptophysin-containing endoplasmic vesicles (EV) to the ciliary band cells. Then, GABA transmitted to the cytoplasm of the CB cells binds to GABAAR near the basal body, and then, GABAAR transmits the signal to GABARAP and tubulin in the cilia of the basal body.

Fig. 9. Katow et al.